

# RSC Advances



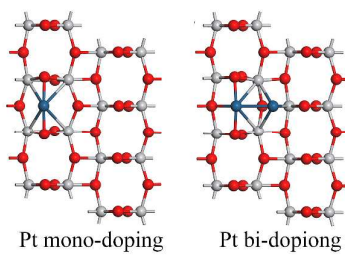
This is an *Accepted Manuscript*, which has been through the Royal Society of Chemistry peer review process and has been accepted for publication.

*Accepted Manuscripts* are published online shortly after acceptance, before technical editing, formatting and proof reading. Using this free service, authors can make their results available to the community, in citable form, before we publish the edited article. This *Accepted Manuscript* will be replaced by the edited, formatted and paginated article as soon as this is available.

You can find more information about *Accepted Manuscripts* in the [Information for Authors](#).

Please note that technical editing may introduce minor changes to the text and/or graphics, which may alter content. The journal's standard [Terms & Conditions](#) and the [Ethical guidelines](#) still apply. In no event shall the Royal Society of Chemistry be held responsible for any errors or omissions in this *Accepted Manuscript* or any consequences arising from the use of any information it contains.

## Table of contents



Pt mono-/bi-doping on anatase  $\text{TiO}_2$  (101) surface are the initial stage of Pt cocatalyst loading onto  $\text{TiO}_2$  photocatalyst surface.

# DFT study on microstructures and electronic structures of Pt mono-/bi-doped anatase TiO<sub>2</sub> (101) surface

Qing-Lu Liu<sup>1,2</sup>, Zong-Yan Zhao<sup>1,\*</sup>

<sup>1</sup> Faculty of Materials Science and Engineering, Key Laboratory of Advanced Materials of Yunnan Province, Kunming University of Science and Technology, Kunming 650093, People's Republic of China

<sup>2</sup> School of Physical Science and Technology, Yunnan University, Kunming 650091, People's Republic of China

\*Corresponding author, E-mail: zzy@kmust.edu.cn. Tel: +86-871-65109952, Fax: +86-871-65107922.

## Abstract

The microstructures and electronic structures of Pt mono- and bi-doped anatase TiO<sub>2</sub> (101) surfaces are investigated by density functional theory calculations, in order to elucidate the surface doping effects and the initial stage of Pt cocatalyst onto TiO<sub>2</sub> photocatalyst surface. Several substitutional and interstitial configurations for the Pt impurity on the surface are studied, and the relative stability of different doping configurations is compared by the impurity formation energy. Under reducing condition, surface interstitial (in other words, surface adsorbed) doping for Pt are more stable than any competitors (substitutional, bulk or subsurface doping) on anatase TiO<sub>2</sub> (101) surface. Compared with bulk doping, the metal induced gap states are very localized and outstanding in the cases of Pt surface interstitial doping onto TiO<sub>2</sub> (101) surface. In the cases of Pt substitutional doping, the surface doping effects are harmful for the photocatalysis due to the metal induced gap states in the middle of band gap. On the contrary, in the case of Pt interstitial doping, the surface doping effects are very favorable for the photocatalysis due to the metal induced gap states overlapping with the top of valance band. Systematic calculations reveal that Pt doping is prone to occupy the interstitial sites on (101) surface. Especially, in the case of Pt bi-doping, two Pt impurity atoms can be co-adsorbed on the surface to form stable configuration, as a result of the strong Pt-Pt atomic interaction. Thus, Pt mono-/bi-doping on anatase TiO<sub>2</sub> (101) surface could be considered as the initial stage (nucleation process) of Pt cocatalyst loading onto TiO<sub>2</sub> photocatalyst surface. Therefore, the calculated results in this work could be considered as the basis of further investigation about Pt<sub>n</sub> cluster loading or Pt/TiO<sub>2</sub> interface forming and water molecule adsorption or decomposition on Pt/TiO<sub>2</sub> composite photocatalyst.

## Keywords

Photocatalysis; Pt cocatalyst; Surface doping; DFT calculations

## 1. Introduction

In the past few decades, the technology of hydrogen generation from photocatalytic water splitting, as one of the most promising and potential renewable energy technologies, has been attracted more and more concerns. However, the solar quantum conversion efficiency is very low, which hinders the further development and industrial application of this technology.<sup>1</sup> In order to promote the photocatalytic activity, researchers attempted to load cocatalysts onto photocatalyst surface to enhance the photocatalytic activity.<sup>2-10</sup> For example, Sato et al. observed the reactivity of hydrogen and oxygen production is enhanced using Pt/TiO<sub>2</sub> composite photocatalyst;<sup>9</sup> Sclafani et al. had loaded Ag particles on TiO<sub>2</sub> surface to improve the hydrogen evolution from the decomposition of alcohol, due to Ag particles capture the photogenerated electrons.<sup>10</sup>

When cocatalyst is loaded onto photocatalyst surface, the photogenerated electron-hole pairs could be spatially separated, because electrons and holes could be respectively localized onto the surfaces of semiconductor and cocatalyst. Consequently, the recombination of photogenerated electron-hole pairs could be inhibited, as well as the oxidation reaction and reduction reaction occur at different surface positions. By this way, the photocatalytic activity and selectivity could be greatly improved. Recently, noble metal cocatalyst loading has been reported to be a suitable cocatalyst, because it can improve the solar quantum conversion efficiency and enhance the light-absorption efficiency. The common noble metals used as cocatalyst in photocatalysis include Ag, Pt, Pd, Au, Ru.<sup>11-16</sup> Pt/TiO<sub>2</sub> composite is the most common system in this field. And, most previous works have confirmed that photogenerated electrons could transfer to Pt nanoparticles.<sup>17-19</sup> Compared with that of pure TiO<sub>2</sub> semiconductor, Pt/TiO<sub>2</sub> composite shows stronger photo-reduction ability. At the same time, the photogenerated holes can freely diffuse at the TiO<sub>2</sub> surfaces, and further photo-oxidize the absorbed organic compounds on the TiO<sub>2</sub> surfaces.<sup>20</sup> Facchin et al. loaded Pt particles on TiO<sub>2</sub> surface by Sol-Gel method, and observed a kind of oxidation of functional groups on the sample surfaces, which enhance the photocatalytic activity of TiO<sub>2</sub>.<sup>21</sup>

Most previous works published in literature demonstrated that tunable photocatalytic activity of Pt cocatalyst loading on TiO<sub>2</sub> surface can be achieved by Pt loading amount and the microstructure of Pt/TiO<sub>2</sub> interface.<sup>22, 23</sup> In addition to Pt nanoparticles loading onto surfaces, Pt surface doping is also another existence way for TiO<sub>2</sub> photocatalyst. The incorporation of Pt atoms onto TiO<sub>2</sub> substrate can be interstitial or substitutional doping as well as being adsorption. Indeed, experiments showed that Pt atoms can thermally diffuse into TiO<sub>2</sub> lattice under oxidizing atmosphere, and be oxidized to Pt<sup>2+</sup> to substitute for Ti<sup>4+</sup> or form the interstitial ions.<sup>24</sup> Some reports have suggested that Pt acts as an electron-hole separation center and therefore inhibit electron-hole recombination at lower amount loading, while Pt acts as electron-hole recombination center at higher amount loading.<sup>12, 25, 26</sup> Importantly, Han et al. used density functional theory (DFT) calculations to investigate the adsorption of Pt cluster on the anatase TiO<sub>2</sub> (101) surface, and demonstrated that Pt<sub>n</sub> favors the coordinately unsaturated step edge sites, which may serve as nucleation sites for the growth of metal clusters on the oxide surface.<sup>27</sup> And then, Gong et al. observed Pt clusters, as small as monomers, on the terraces of anatase TiO<sub>2</sub> (101) surface with large binding energy, using DFT calculations and room-temperature scanning tunneling microscopy (STM) measurements;<sup>19</sup> Zhou et al. also considered that Pt prefers to form 3-D rather 2-D structures or monolayers on the anatase TiO<sub>2</sub> (101) surface.<sup>28</sup> Similar phenomena and characteristics are observed for Pd cluster on anatase TiO<sub>2</sub> (101) surface.<sup>29</sup>

However, above important works mainly considered the growth mechanism of Pt<sub>n</sub> cluster on the

anatase TiO<sub>2</sub> (101) surface. To the best of our knowledge, there are few detailed reports on the electronic properties of Pt-doped TiO<sub>2</sub> surfaces, revealing the physical and chemical origin of the enhanced photocatalytic performance of Pt/TiO<sub>2</sub> composite photocatalyst, until now. Furthermore, the surface doping could be considered as the initial stage for the Pt<sub>n</sub> cluster loading or Pt/TiO<sub>2</sub> interface formation, which means the microstructure and properties will determine the subsequent stages. In our previous work, we have been systematically investigated the overall evolutionary process of Pt cocatalyst loading on anatase TiO<sub>2</sub> (101) surface and the related microstructure and properties. We found that the growth of Pt cocatalyst on anatase TiO<sub>2</sub> (101) surface sequentially experiences the following stages: surface doping, cluster nucleating, cluster loading, one-dimensional nanowire loading, two-dimensional nanowire grid loading, ultrathin film ripening, and film forming via the layer-by-layer mode, with the increase of loading amount. And in this growth process, Pt surface doping is very crucial for the subsequent stages.<sup>30</sup> In order to further improve the fundamental understanding of Pt/TiO<sub>2</sub> composite photocatalyst, and provide helpful information about the relationship between surface doping and photocatalytic performance, we chosen Pt mono- and bi-doped anatase TiO<sub>2</sub> (101) surface as research object, and adopted DFT calculations as research method to investigate their microstructure and electronic structure in the present work. We believe that the findings are crucial for further research on these noble metal-TiO<sub>2</sub> composite photocatalyst for practical applications.

## 2. Computational methods and models

The TiO<sub>2</sub> (101) surface was simulated by a (2×3) periodic slab of 12 O-Ti-O trilayers (72 TiO<sub>2</sub> units, 216 atoms). And, the slab model was separated by a 20-Å-thick vacuum layer. The lengths of the model along [10 $\bar{1}$ ], [010] and [101] directions were 11.0092, 11.3235, and 65 Å, respectively. Thus, all the lengths of the model were larger than 10 Å, which were enough to avoid the self interaction effects of the periodic boundary conditions. The bottom half of the slab was fixed to mimic the bulk effects. For the substitutional models, one or two Ti atoms were replaced by Pt atoms, while one or two Pt atoms were placed at the interstice sites of the surface for the interstitial models. In order to compare the similarity and difference between surface doping and bulk doping, a 3×3×1 supercell model was constructed for Pt bulk doping.

In the present study, all of DFT calculations have been carried out by using Cambridge Serial Total Energy Package (CASTEP) codes, employing the ultrasoft pseudopotential.<sup>31</sup> Exchange and correlation effects were described by the revised Perdew-Burke-Ernzerhof for solid (PBEsol) of generalized gradient approximation (GGA).<sup>32</sup> An energy cutoff of 340 eV has been used for expanding the Kohn-Sham wave functions. The minimization algorithm has been chosen Broyden-Fletcher-Goldfarb-Shanno (BFGS) scheme.<sup>33</sup> The K-points grid sampling of Monkhorst-Pack scheme was set as 1×1×1 in the irreducible Brillouin zone, and the fast Fourier transform grid was set as 60×60×360. To get accurate results, we optimized atomic coordinates, which obtained by minimizing the total energy and atomic forces. This was done by performing an iterative process in which the coordinates of the atoms are adjusted so that the total energy of the structure is minimized. The relaxation run was considered converged when the force on the atomic nuclei was less than 0.03 eV/Å, the stress on the atomic nuclei was less than 0.05 GPa, the displacement of the nuclei was less than 1×10<sup>-3</sup> Å, and the energy change per atom was less than 1×10<sup>-5</sup> eV. In order to improve accuracy of calculated adsorption energies for Pt atoms on TiO<sub>2</sub> (101) surface, the dipole corrections were utilized for all models, which can be essential in eliminating nonphysical

electrostatic interaction between periodic images.<sup>34</sup> In order to get accurate electronic structure, the GGA+U method were further adopted to overcome the well-known shortcoming of GGA. The U value of 4.2 eV was applied to the Ti-d states, Pt-d states and the O-p states. Using these values, the accurate band gap of anatase TiO<sub>2</sub> (3.209 eV) could be obtained that could be compared with experimental measurements, as well as keeping the main features of electronic structure obtained by the standard DFT calculations.

Using the above calculation method, we first optimized the bulk crystal structure of anatase TiO<sub>2</sub>, and obtained the following lattice constants:  $a = b = 3.7747 \text{ \AA}$ ,  $c = 9.6289 \text{ \AA}$ ,  $d_{\text{ap}} = 1.9898 \text{ \AA}$ ,  $d_{\text{eq}} = 1.9329 \text{ \AA}$ ,  $2\theta = 155.058^\circ$ . This calculation results is well consistent with the experimental measurements:<sup>35</sup>  $a = b = 3.7848 \text{ \AA}$ ,  $c = 9.5124 \text{ \AA}$ ,  $d_{\text{ap}} = 1.9799 \text{ \AA}$ ,  $d_{\text{eq}} = 1.9338 \text{ \AA}$ ,  $2\theta = 156.230^\circ$ . Then, we optimized the structure of perfect TiO<sub>2</sub> (101) surface using above calculation method, obtaining the surface configuration that is well consistent with previous reports.<sup>36, 37</sup> On the other hand, the lattice constants of fcc Pt metal is  $4.0043 \text{ \AA}$ . These calculated results indicate that the calculation models and method in the present work are reasonable.

### 3. Results and discussions

#### 3.1 Single Pt atom surface doping

When Pt atoms adsorbed onto TiO<sub>2</sub> surface, they not only likely occupy the topmost adsorption sites, but also may diffuse to the regime below the surface. In other words, for Pt surface mono-doping, not only there exists a possibility of substitutional or interstitial doping for the topmost surface atoms, but also there exists a certain possibility of substitutional or interstitial doping for the subsurface atoms. Thus, in the section, we firstly investigated the doping effects of a single Pt atom on the anatase TiO<sub>2</sub> (101) surface. For this purpose, various possible nonequivalent surface and subsurface doping positions were considered. To examine the relative difficulty for different doping configurations, the impurity formation energy ( $E_f$ ) for every doping system were calculated, according to the following equation that is defined by Van de Walle et al., which is a widely accepted method to compare the relative degree of difficulty or solubility of impurity incorporate to host lattice.<sup>38</sup>

$$E_f = E_{\text{Pt/TiO}_2} - E_{\text{TiO}_2} - n\mu_{\text{Pt}} + m\mu_{\text{Ti}} \quad (\text{Eq. 1})$$

where  $E_{\text{Pt/TiO}_2}$  is the total energy of Pt-doped TiO<sub>2</sub> system (bulk or surface);  $E_{\text{TiO}_2}$  is the total energy of pure TiO<sub>2</sub> system (bulk or surface), which has the same corresponding atom numbers with doping system.

$\mu_{\text{Pt}}$  and  $\mu_{\text{Ti}}$  is the chemical potential of Pt and Ti.  $n$  is the number of Pt doping atoms;  $m$  is the number of replaced Ti atoms. The chemical potentials depend on the experimental growth conditions (oxidizing conditions or reducing conditions). For pure TiO<sub>2</sub>,  $\mu_{\text{Ti}}$  and  $\mu_{\text{O}}$  satisfy the relationship:

$\mu_{\text{Ti}} + 2\mu_{\text{O}} = E_{\text{TiO}_2}$ . Under extreme oxidizing conditions,  $2\mu_{\text{O}}$  is the total energy of O<sub>2</sub> molecule in gas

phase; while under extreme reducing conditions,  $\mu_{\text{Ti}}$  is the total energy of bulk metal of Ti. And in the present work,  $\mu_{\text{Pt}}$  is the total energy of bulk metal of Pt. In practice, the preparation of Pt doping usually

carry out between these two extremes, suggesting that the final doping configuration of Pt will depend on synthesis condition as well as after-preparation treatments. The impurity formation energies under reducing conditions are plotted in shown in Figure 1.

Under reducing condition, Pt interstitial doping is favored over substitutional doping on anatase TiO<sub>2</sub> (101) surface. For Pt interstitial doping, the impurity formation energy is first increasing, and then decreasing with the increase of distance of Pt impurity from the surface. The most stable interstitial position is the hollow site between two bridging O<sub>2c</sub> atoms as shown in Figure 2(a). On the contrary, the impurity formation energy of Pt substitutional doping is decreasing as a function of distance from the surface. The most stable substitutional position is to replace Ti<sub>6c</sub> atom in the second trilayer below the surface about 5.053 Å. Owing to the relaxation constraint along the directions parallel to the surface, so the value of E<sub>f</sub> for surface system is larger than that of the corresponding bulk doping systems. It is particularly noteworthy that E<sub>f</sub> of Pt doping at the hollow site (in other words, Pt adsorb onto this position) is much lower than the E<sub>f</sub> of all other doping positions, even lower than the E<sub>f</sub> of bulk doping system. This result implies that Pt atoms are more easily enriched on TiO<sub>2</sub> (101) surface when the sample is prepared under reducing conditions. The most stable doping configurations of Pt in the present work are identical with previous theoretical works.<sup>19, 27, 28</sup> In order to explore the modification effect of Pt on TiO<sub>2</sub> (101) surface for the water adsorption and decomposition (which is ongoing by our group at present), we only considered the doping effect of Pt on the topmost of surface (as shown in Figure 2) in the following sections.

The electronic structure of Pt-doped anatase TiO<sub>2</sub> (bulk and (101) surface) in different forms is shown in Figure 3. For both bulk doping, the impurity energy bands are mainly consisted by the hybridization between Pt-5d states and O-2p states, and they are located at the top and bottom of valence band (VB). What's more, these impurity energy bands are overlapping with the top or bottom of VB. The main difference between them is shown by the effect of Fermi energy level (E<sub>F</sub>) shifting: E<sub>F</sub> more obviously shift upward, even moves into the bottom of conduction band (CB), in the case of interstitial doping. For Pt substitutional doping on TiO<sub>2</sub> surface, there is an isolated impurity energy band in the middle of the band gap, which is predominantly consisted of Pt-5d states. These impurity energy bands could be considered as the metal induced gap states (MIGS). This type of impurity energy band could become the recombination center of photogenerated electron-hole pairs. And, the impurity energy bands at the top or bottom of VB are more prominent, compared with Pt substitutional doping in bulk TiO<sub>2</sub>. For Pt interstitial doping on TiO<sub>2</sub> surface, there are three differences compared with Pt interstitial doping in bulk TiO<sub>2</sub> as following: the impurity energy band located at the top of VB is also more prominent, while the impurity energy band located at the bottom of VB is disappeared, and the E<sub>F</sub> is located at the top of impurity energy band. The major advantage of this type doping is the realization of visible-light absorption, in which two lower-energy photons successfully excite one electron from VB to impurity energy band, and then to CB.

As shown in Figure 4, the direction of electrons transfer could be well described by the maps of electron density difference. Compared with pure TiO<sub>2</sub> (bulk or surface), the oxygen atoms that are neighboring with Pt atom obtain more electrons. In other words, Pt atom loses more electrons than Ti atoms. However, there is an exception that the bridging O<sub>2c</sub> atoms bonded with Pt atom do not get more electrons and the Pt atom only loses a few electrons in the case of Pt interstitial doping on surface. Either bulk doping or surface doping, the neighboring O atoms bonded with Pt get more electrons in the case of Pt substitutional doping than that of Pt interstitial doping. Thus, in this type of doping case, the interaction of Pt atom with neighboring O atoms is relatively stronger. Furthermore, in these figures, it is observed that the doping effect of Pt is rather localized and gradually disappears as the distance increasing with the Pt atom. This implies that Pt dopant only influence the electronic states of neighboring atoms and the local

crystal or surface structure.

### 3.2 Double Pt atoms surface doping

Due to the larger ionic radius of Pt, double Pt atoms doping is very difficult to incorporate into bulk TiO<sub>2</sub> host, neither substitutional nor interstitial doping. Furthermore, in practical photocatalysis, Pt is usually deposited onto TiO<sub>2</sub> surface as cocatalyst. Thus, in this subsection, we only considered Pt surface doping. For double Pt atoms surface doping, we considered three types of model: both substitutional doping, one substitutional doping plus one interstitial doping, and both interstitial doping. The corresponding  $E_f$  under reducing condition is shown in Figure 5. On the (101) surface, the variations of  $E_f$  as function of dopants' distance are all very small on the whole surface. When the distance between two Pt atoms is increasing, the situation of these three types of doping is similar with the single Pt atom doping. For these models, the values of  $E_f$  are decreased as the decrease of dopants' distance, implying the existence of strong Pt-Pt atomic interaction. As well as Pt mono-doping, the values of  $E_f$  of both interstitial bi-doping is much lower than that of other two bi-doping ways under reducing condition. Moreover, it is negative, implying the preparation process is an exothermic reaction. Since Pt atoms as the added atoms are deposited onto the surface in the practical sample preparation, so in the most cases the most possible results are surface adsorbing (or surface interstitial doping), nanoparticles loading, and interface forming. Furthermore,  $E_f$  value is significantly decreased when the distance between Pt atoms is less than 2.7 Å. At this distance, Pt atoms could be bonded together, resulting from the Pt-Pt atomic interaction. So, Pt interstitial bi-doping can be seen as the process of nucleation of Pt cocatalyst on anatase TiO<sub>2</sub> (101) surface.

Figure 6 shows the electronic structure of each stable configuration of three doping ways. In the case of both substitutional doping as shown in Figure 6(a), the most stable configuration is one Pt atom replaces the Ti<sub>5c</sub> atom and other Pt atom replaces the neighboring Ti<sub>6c</sub> atom in the second trilayer. The distance between Pt atoms is 3.05 Å. There is an isolated impurity energy band in the middle of band gap, which is formed by the hybridization of Ti<sub>5c</sub>-5d states with O<sub>2c</sub>-2p states. At the top of VB, there is an impurity energy band overlapped with VB, which is mainly consisted with Ti<sub>5c</sub>-5d states, Ti<sub>6c</sub>-5d states, and O<sub>2c</sub>-2p states. While, at the bottom of CB, there is an impurity energy band overlapped with CB, which is formed by the hybridization of Ti<sub>6c</sub>-5d states with O<sub>2c</sub>-2p states. And, at the bottom of VB, there is also another impurity energy band that is mainly consisted with Ti<sub>5c</sub>-5d states, Ti<sub>6c</sub>-5d states, and O<sub>2c</sub>-2p states. In the case of one substitutional doping plus one interstitial doping as shown in Figure 6(b), the most stable configuration is one Pt atom replaces the Ti<sub>5c</sub> atom and other Pt atom occupies the neighboring hollow site between two bridging O<sub>2c</sub> atoms. The distance between Pt atoms is 2.779 Å. At the top of CB, there are two impurity energy bands. The lower band is mainly formed by the hybridization of interstitial Pt-5d states with O<sub>2c</sub>-2p states, and the higher band is mainly formed by the hybridization of substitutional Pt-5d states with O<sub>2c</sub>-2p states. At the bottom of CB, there is another impurity energy band that is almost isolated. It is mainly consisted by interstitial Pt-5d states, substitutional Pt-5d states and O<sub>2c</sub>-2p states. The impurity energy band at the bottom of VB is relatively weakened. The most stable configuration for the case of both interstitial doping were described above as shown in Figure 2(b), and the corresponding electronic structure as shown in Figure 6(c). In this case, there is only one impurity energy band at the top of VB, which is mainly consisted by Pt<sub>H</sub>-5d states, and the hybridization of Pt<sub>L</sub>-5d states with O<sub>2c</sub>-2p states. In the band gap and the bottom of VB, there are no any impurity energy bands. Similarly, the  $E_f$  positions are relatively upward shifting in the latter two cases, because of interstitial Pt atoms doping. Compared with Pt interstitial mono- and bi-doping, one could found that the similar impurity energy band on the top of VB. Thus, the

Pt-Pt atomic interaction enhances the advantage of Pt interstitial doping for the photocatalytic activity as mentioned above.

The results of electron density difference as shown in Figure 7 are again confirmed the conclusion that the electron transfer is more prominent for the local atoms around Pt dopant. In the first case of both substitutional doping, Pt atoms loses more electrons than that of  $Ti_{5c}$  or  $Ti_{6c}$  atoms, and their neighboring  $O_{3c}$  atoms get more electrons as shown in Figure 7(a). However, the  $O_{2c}$  atoms that bonded with Pt atom do not seem to get more electrons. Instead, the number of transferred electron to them is slightly less than that of other bridging  $O_{2c}$  atoms on the surface. On the contrary, the number of transferred electron to them is obvious more than that of other bridging  $O_{2c}$  atoms on the surface in the latter two cases as shown in Figure 7(b) and Figure 7(c). In the second case of one substitutional doping plus one interstitial doping, the electron transfer of substitutional Pt atom is more obvious than that of interstitial Pt atom. And, in the case of both interstitial doping, the electron transfer of lower Pt atom is also more obvious than that of higher Pt atom. With different types of impurity energy bands and different modes of electron transfer, the transfer process of photogenerated carriers from  $TiO_2$  substrate to Pt cocatalyst will be differently influenced.

## 4. Conclusions

For Pt cocatalyst loading onto anatase  $TiO_2$  (101) surface, its cocatalyst effects present more the characteristics of surface doping, at the very lower coverage. Firstly, it is found that surface interstitial (in other words, surface adsorbed) doping for Pt are more stable than any competitors (substitutional, bulk or subsurface doping) on anatase  $TiO_2$  (101) surface, under reducing condition. In the case of Pt bi-doping, two Pt impurity atoms can be co-adsorbed on the surface to form stable configuration, as a result of the strong Pt-Pt atomic interaction. Thus, Pt mono- and bi-doping on anatase  $TiO_2$  (101) surface could be considered as the initial stage (nucleation process) of Pt cocatalyst loading onto  $TiO_2$  photocatalyst surface. In the cases of Pt interstitial surface doping, the metal induced gap states of Pt are very localized and outstanding. In the cases of Pt substitutional doping, the surface doping effects are harmful for the photocatalysis due to the metal induced gap states in the middle of band gap. On the contrary, in the cases of Pt interstitial doping, the surface doping effects are very favorable for the photocatalysis due to the metal induced gap states overlapping with the top of valence band. And, the major advantage of Pt interstitial surface doping is the realization of visible-light absorption, in which two lower-energy photons successfully excite one electron from valence band to impurity energy band, and then to conduction band. Based on these calculated results, one could further investigate the  $Pt_n$  cluster loading or Pt/ $TiO_2$  interface forming, and the surface doping effects on the water adsorption and decomposition, which works are carrying out in our group.

## Acknowledgments

The authors would like to acknowledge financial support from the National Natural Science Foundation of China (Grant No.21263006).

## References

1. A. Kudo and Y. Miseki, *Chem. Soc. Rev.*, 2009, **38**, 253.

2. J. Yang, D. Wang, H. Han and C. Li, *Accounts. Chem. Res.*, 2013, **46**, 1900.
3. G. N. Schrauzer and T. D. Guth, *J. Am. Chem. Soc.*, 1977, **99**, 7189.
4. S. Sato and J. M. White, *J. Phys. Chem.*, 1981, **85**, 592.
5. A. V. Bulatov and M. L. Khidekel, *Russ. Chem. Bull.*, 1976, **25**, 1794.
6. G. R. Bamwenda, S. Tsubota, T. Nakamura and M. Haruta, *J. Photoch. Photobio. A*, 1995, **89**, 177.
7. V. Subramanian, E. Wolf and P. V. Kamat, *J. Phys. Chem. B*, 2001, **105**, 11439.
8. M. Jakob, H. Levanon and P. V. Kamat, *Nano Lett.*, 2003, **3**, 353.
9. S. Sato and J. M. White, *Chem. Phys. Lett.*, 1980, **72**, 83.
10. A. Sclafani, M.-N. Mozzanega and P. Pichat, *J. Photoch. Photobio. A*, 1991, **59**, 181.
11. N. Sobana, M. Muruganadham and M. Swaminathan, *J. Mol. Catal. A: Chem.*, 2006, **258**, 124.
12. G. N. Kryukova, G. A. Zenkovets, A. A. Shutilov, M. Wilde, K. Günther, D. Fassler and K. Richter, *Appl. Catal. B*, 2007, **71**, 169.
13. L. Ge, M. Xu and H. Fang, *Appl. Surf. Sci.*, 2006, **253**, 2257.
14. Z. Bian, T. Tachikawa, P. Zhang, M. Fujitsuka and T. Majima, *J. Am. Chem. Soc.*, 2014, **136**, 458.
15. K. T. Ranjit, T. K. Varadarajan and B. Viswanathan, *J. Photoch. Photobio. A*, 1995, **89**, 67.
16. K. Drew, G. Girishkumar, K. Vinodgopal and P. V. Kamat, *J. Phys. Chem. B*, 2005, **109**, 11851.
17. Z. Zhang and J. T. Yates, *Chem. Rev.*, 2012, **112**, 5520.
18. H. Tada, T. Kiyonaga and S.-i. Naya, *Chem. Soc. Rev.*, 2009, **38**, 1849.
19. X.-Q. Gong, A. Selloni, O. Dulub, P. Jacobson and U. Diebold, *J. Am. Chem. Soc.*, 2008, **130**, 370.
20. K. Hiehata, A. Sasahara and H. Onishi, *Nanotechnology*, 2007, **18**, 084007.
21. G. Facchin, G. Carturan, R. Camprostrini, S. Gialanella, L. Lutterotti, L. Armelao, G. Marci, L. Palmisano and A. Sclafani, *J. Sol-gel. Sci. Techn.*, 2000, **18**, 29.
22. D. R. Jennison, O. Dulub, W. Hebenstreit and U. Diebold, *Surf. Sci.*, 2001, **492**, L677.
23. T. Tamura, S. Ishibashi, K. Terakura and H. Weng, *Phys. Rev. B*, 2009, **80**, 195302.
24. M. Zhang, Z. Jin, Z. Zhang and H. Dang, *Appl. Surf. Sci.*, 2005, **250**, 29.
25. B. K. Vijayan, N. M. Dimitrijevic, J. Wu and K. A. Gray, *J. Phys. Chem. C*, 2010, **114**, 21262.
26. F. Han, V. S. R. Kambala, M. Srinivasan, D. Rajarathnam and R. Naidu, *Appl. Catal. A*, 2009, **359**, 25.
27. Y. Han, C.-j. Liu and Q. Ge, *J. Phys. Chem. B*, 2006, **110**, 7463.
28. Y. Zhou, C. L. Muhich, B. T. Neltner, A. W. Weimer and C. B. Musgrave, *J. Phys. Chem. C*, 2012, **116**, 12114.
29. J. Zhang, M. Zhang, Y. Han, W. Li, X. Meng and B. Zong, *J. Phys. Chem. C*, 2008, **112**, 19506.
30. Z.-Y. Zhao, *J. Phys. Chem. C*, 2014, **118**, 24591.
31. S. J. Clark, M. D. Segall, C. J. Pickard, P. J. Hasnip, M. J. Probert, K. Refson and M. C. Payne, *Z. Kristallogr.*, 2005, **220**, 567.
32. J. P. Perdew, A. Ruzsinszky, G. I. Csonka, O. A. Vydrov, G. E. Scuseria, L. A. Constantin, X. Zhou and K. Burke, *Phys. Rev. Lett.*, 2008, **100**, 136406.
33. B. G. Pfrommer, M. Côté, S. G. Louie and M. L. Cohen, *J. Comput. Phys.*, 1997, **131**, 233.
34. J. Neugebauer and M. Scheffler, *Phys. Rev. B*, 1992, **46**, 16067.
35. J. K. Burdett, T. Hughbanks, G. J. Miller, J. W. Richardson and J. V. Smith, *J. Am. Chem. Soc.*, 1987, **109**, 3639.
36. M. Lazzeri, A. Vittadini and A. Selloni, *Phys. Rev. B*, 2001, **63**, 155409.
37. Z. Zhao, Z. Li and Z. Zou, *J. Phys.: Condens. Matter*, 2010, **22**, 175008.
38. C. G. Van de Walle and J. Neugebauer, *J. Appl. Phys.*, 2004, **95**, 3851.

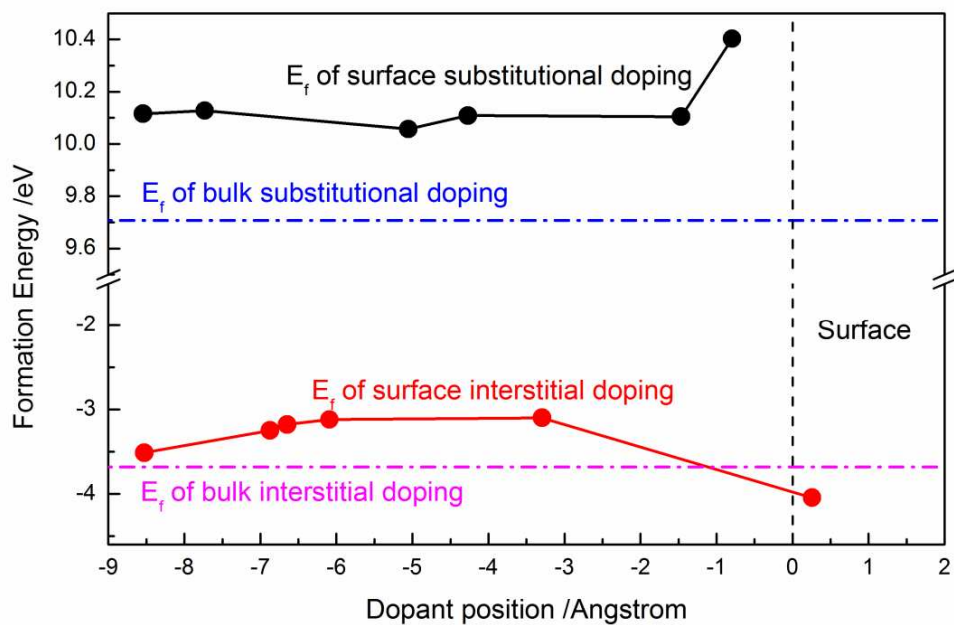


Figure 1. The impurity formation energy of single Pt mono-doping on anatase  $\text{TiO}_2$  (101) surface on different doping positions under reducing condition.

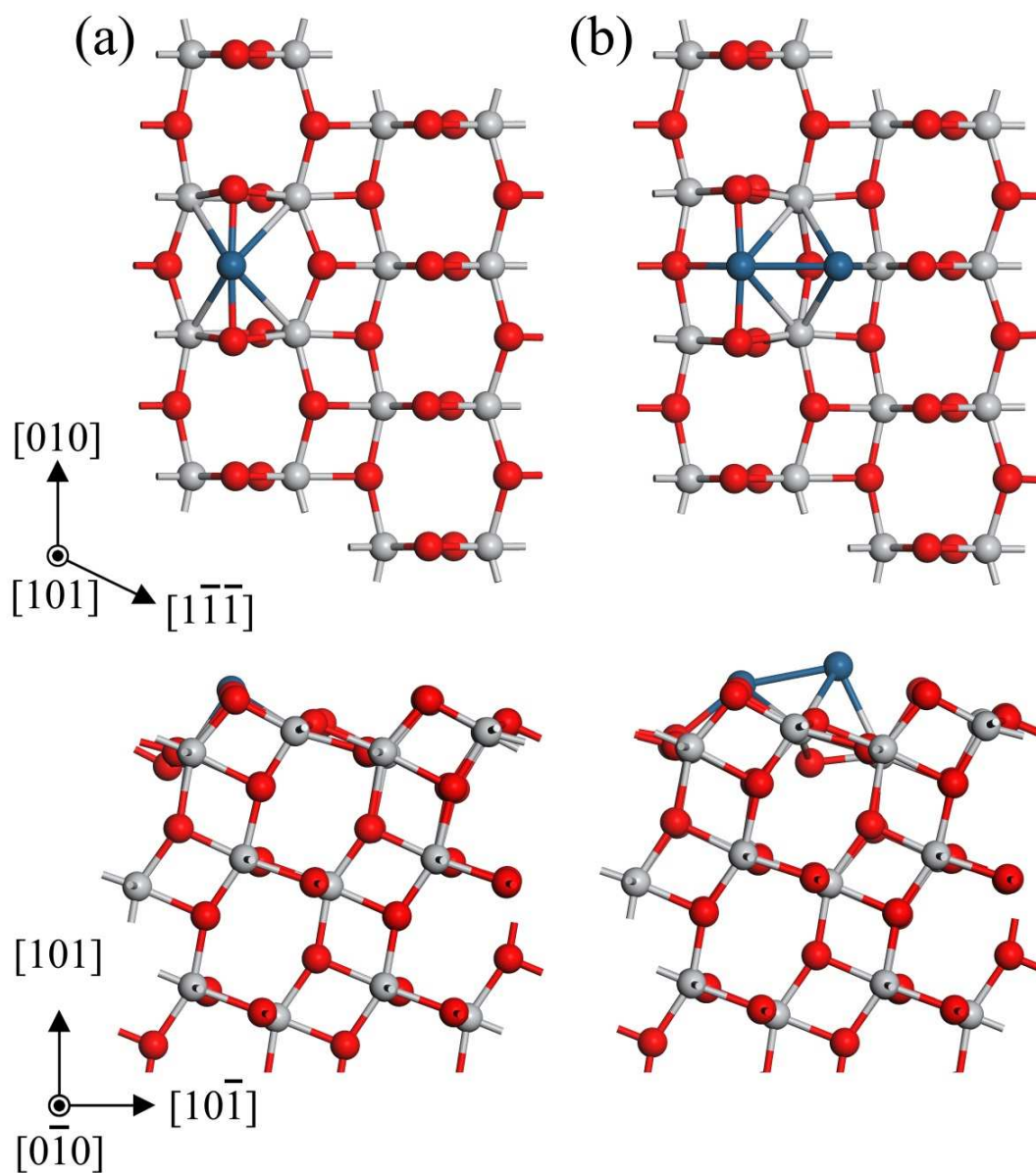


Figure 2. Top view (upper plane) and side view (lower plane) of stable models for: (a) Pt mono-doping; (b) Pt bi-doping. The red balls represent oxygen atoms; the grey balls represent titanium atoms; the navy balls represent platinum atoms. The top view only shows the top two O-Ti-O trilayers.

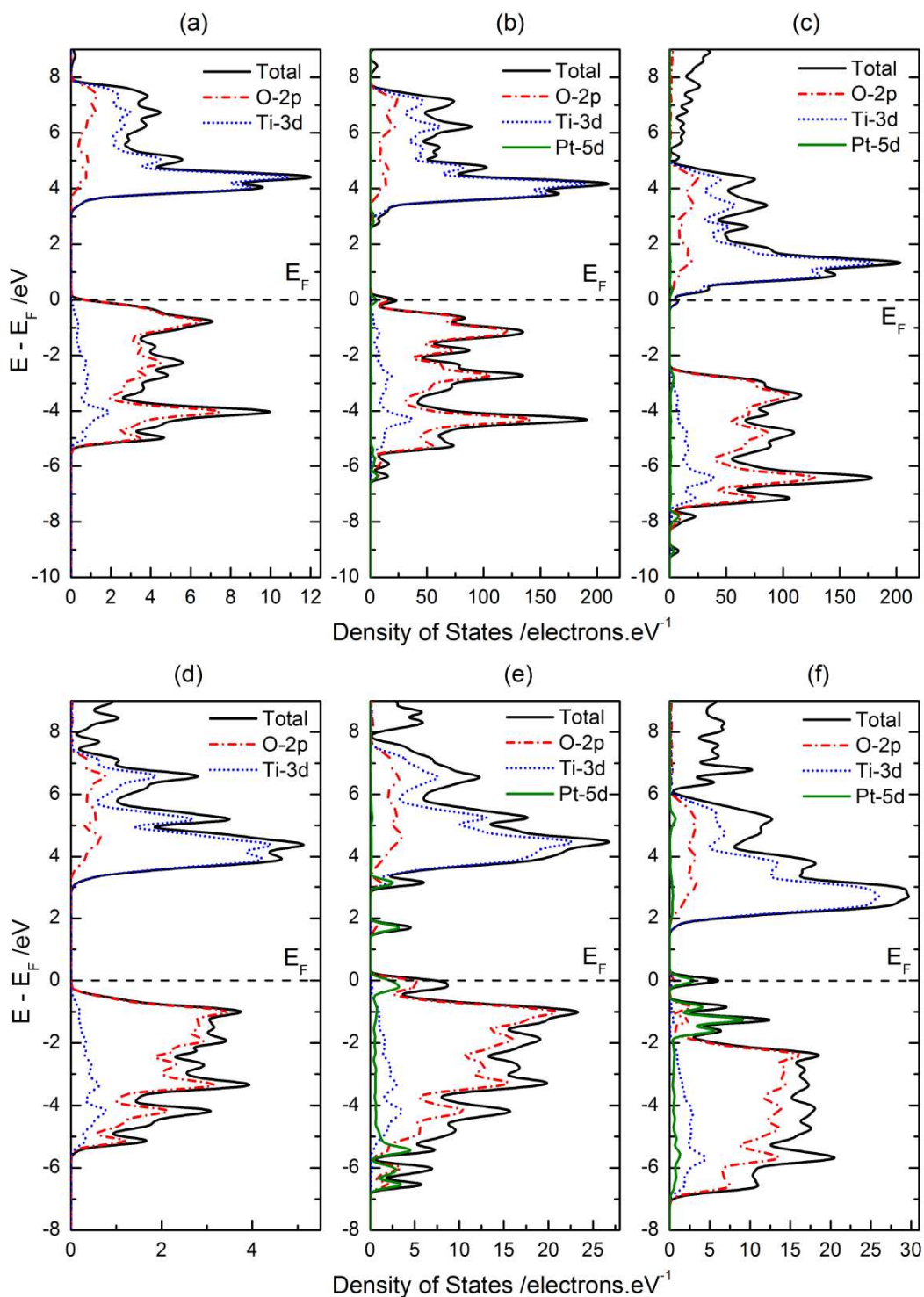


Figure 3. The local and partial density of states of Pt mono-doped anatase  $\text{TiO}_2$ : (a) pure bulk anatase  $\text{TiO}_2$ ; (b) Pt substitutional doped into bulk anatase  $\text{TiO}_2$ ; (c) Pt interstitial doped into bulk anatase  $\text{TiO}_2$ ; (d) pure anatase  $\text{TiO}_2$  (101) surface; (e) Pt substitutional doped into anatase  $\text{TiO}_2$  (101) surface; (c) Pt interstitial doped into anatase  $\text{TiO}_2$  (101) surface. The Fermi energy level ( $E_F$ ) is located at 0 eV.

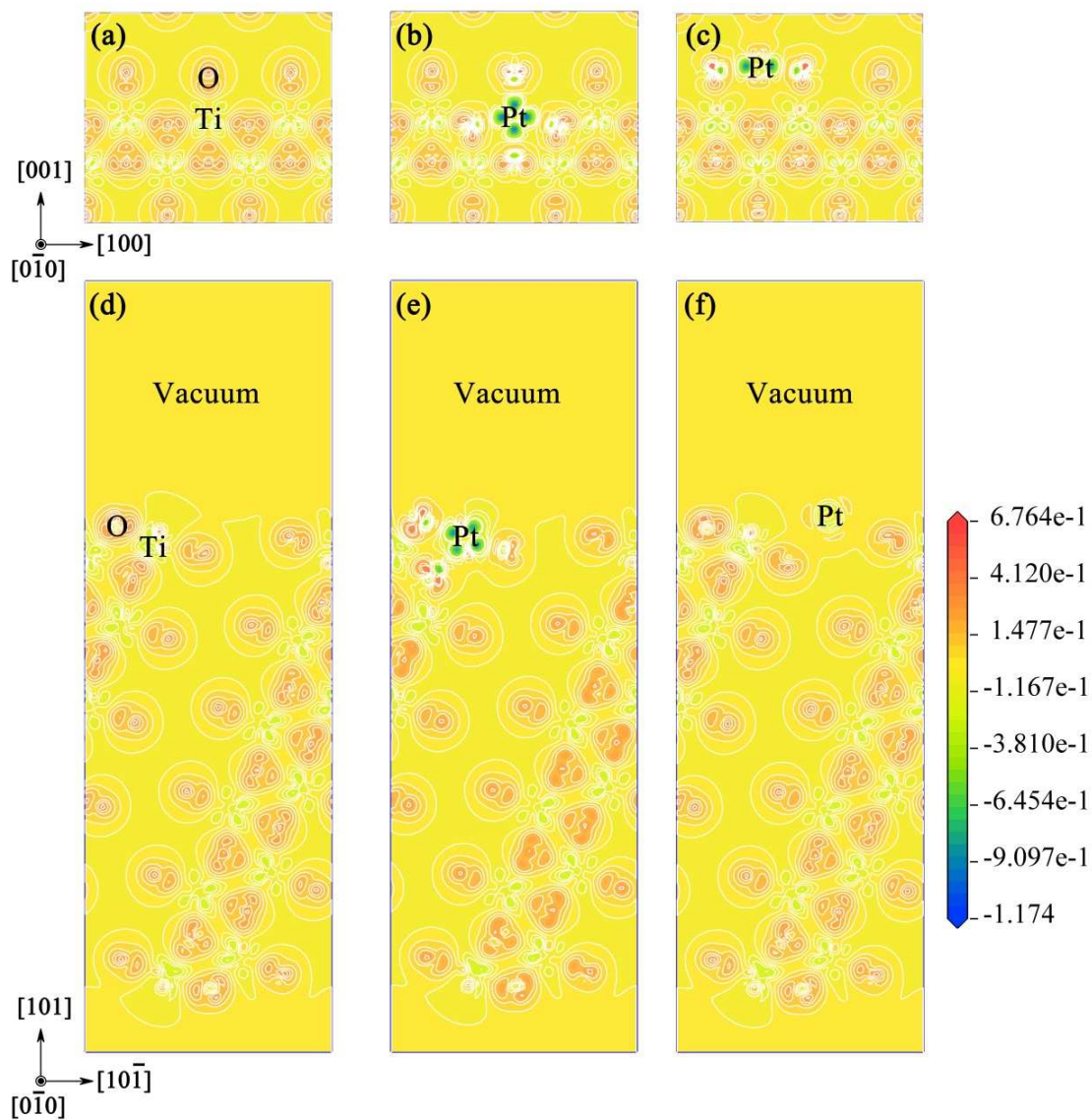


Figure 4. The electron density difference of Pt mono-doped anatase  $\text{TiO}_2$ : (a) pure bulk anatase  $\text{TiO}_2$ ; (b) Pt substitutional doped into bulk anatase  $\text{TiO}_2$ ; (c) Pt interstitial doped into bulk anatase  $\text{TiO}_2$ ; (d) pure anatase  $\text{TiO}_2$  (101) surface; (e) Pt substitutional doped into anatase  $\text{TiO}_2$  (101) surface; (f) Pt interstitial doped into anatase  $\text{TiO}_2$  (101) surface.

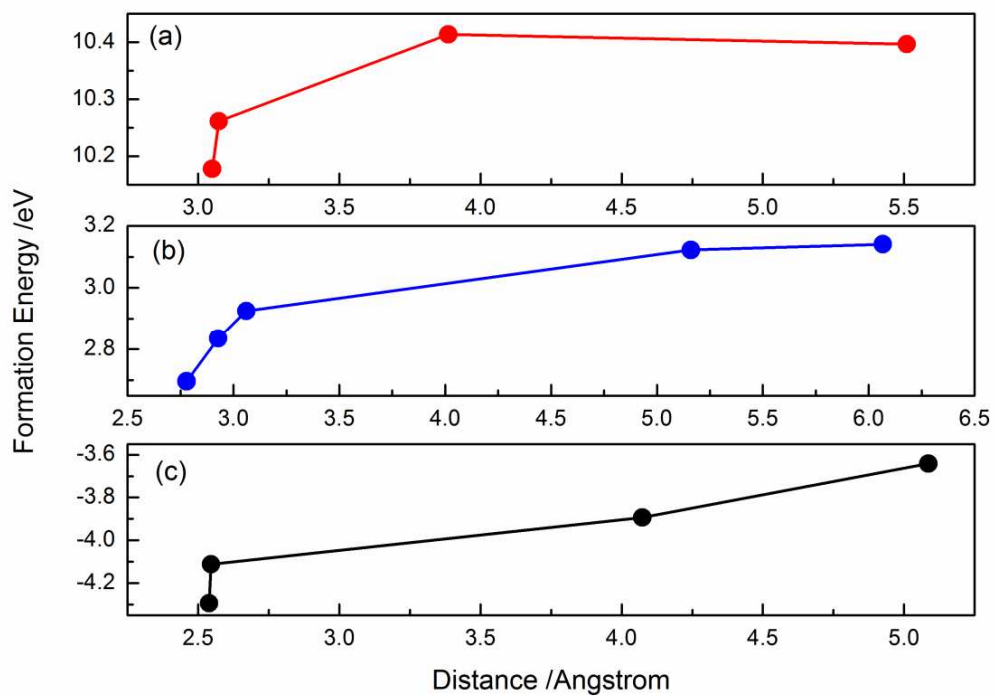


Figure 5. The impurity formation energy of Pt bi-doping on anatase TiO<sub>2</sub> (101) surface as function of the distance between dopants under reducing condition: (a) both substitutional doping; (b) one substitutional doping, and other interstitial doping; (c) both interstitial doping.

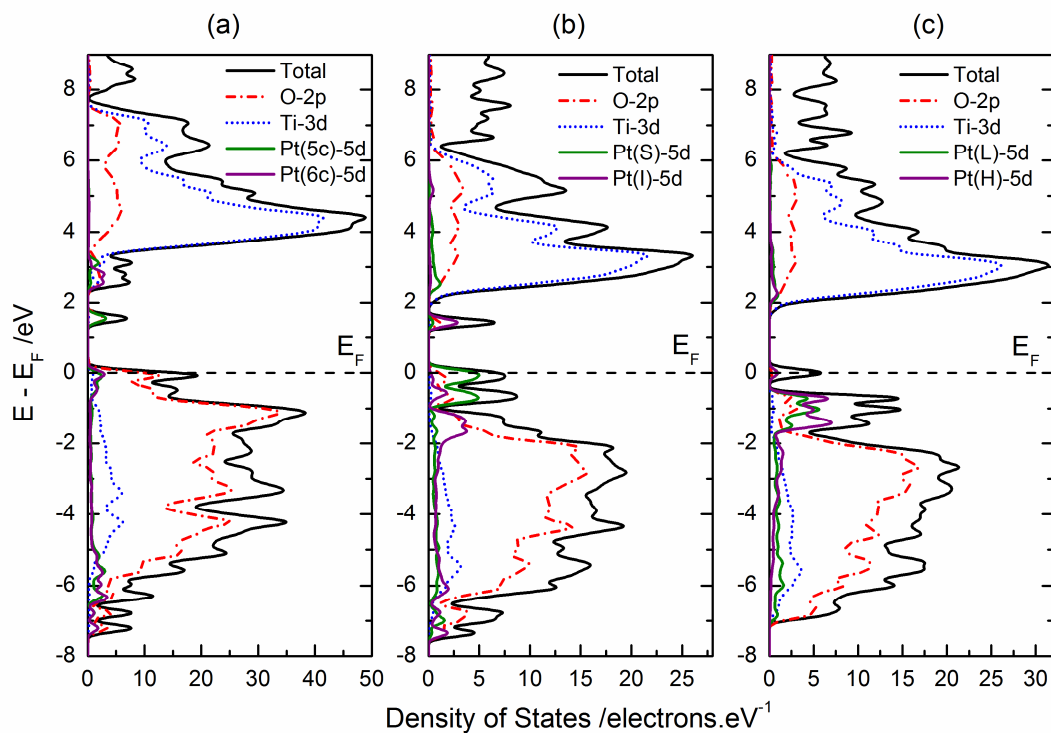


Figure 6. The local and partial density of states of Pt bi-doped onto anatase  $\text{TiO}_2$  (101) surface: (a) both substitutional doping; (b) one substitutional doping, and other interstitial doping; (c) both interstitial doping.

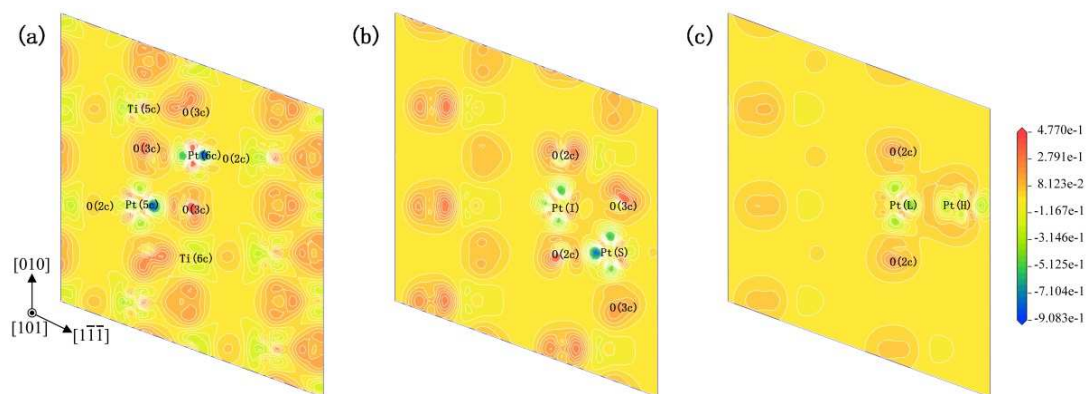


Figure 7. The electron density difference of Pt bi-doped onto anatase TiO<sub>2</sub>: (a) both substitutional doping; (b) one substitutional doping, and other interstitial doping; (c) both interstitial doping.